An Organic Ferroelectric Synaptic Transistor

Zhenyu Feng(冯振语)[1,2†], Jiahao Wu(邬嘉豪)[1,2†], Weihong Yang(杨伟弘)[3†], Wei Li(李伟)[1,2], Guangdi Feng(冯光迪)[1,2], Qiuxiang Zhu(朱秋香)[1,2], Xiangjian Meng(孟祥建)[5*], Xiaojun Guo(郭小军)[3*], Bobo Tian(田博博)[1,2,4*], Junhao Chu(褚君浩)[1,2], and Chungang Duan(段纯刚)[1,2,6]

[1]*Key Laboratory of Polar Materials and Devices (MOE), Ministry of Education, Department of Electronics, East China Normal University, Shanghai 200241, China*
[2]*Shanghai Center of Brain-inspired Intelligent Materials and Devices, Shanghai 200241, China*
[3]*Department of Electronic Engineering, Shanghai Jiao Tong University, Shanghai 200240, China*
[4]*Chongqing Key Laboratory of Precision Optics, Chongqing Institute of East China Normal University, Chongqing 401120, China*
[5]*National Laboratory for Infrared Physics, Shanghai Institute of Technical Physics, Chinese Academy of Sciences, Shanghai 200083, China*
[6]*Collaborative Innovation Center of Extreme Optics, Shanxi University, Shanxi 030006, China*

(Received 7 March 2025; accepted manuscript online 14 April 2025)

Poly(vinylidene-trifluoroethylene) [P(VDF-TrFE)] copolymer films generally demonstrate limited compatibility with organic semiconductors. The material is frequently compromised by exposure to organic semiconductor solutions and other fabrication processes utilized in the production of organic ferroelectric transistors. In this study, an organic ferroelectric field effect transistor (OFeFET) with the 6,13-Bis(triisopropylsilylethynyl) pentacene (TIPS-pentacene) channel is fabricated, in which the aluminum oxide (Al_2O_3) interlayer is used to improve compatibility. The device displays polymorphic memory and synaptic plasticity of long-term potentiation and depression. Furthermore, an artificial neural network constructed using our devices is simulated to succeed in recognizing the MNIST handwritten digit database with a high accuracy of 92.8%. This research offers a viable approach to enhance the compatibility of the organic ferroelectric polymer P(VDF-TrFE) with organic semiconductors.

DOI: 10.1088/0256-307X/42/5/056302 CSTR: 32039.14.0256-307X.42.5.056302

Currently, the development of neuromorphic devices has continued to advance toward high performance, multifunctionality, and high integration.[1–3] Neuromorphic devices with two- or three-terminal structures are used in information storage and computation by modulating carrier transport, which can be classified according to the device structure as floating gate, electrolyte gated, ferroelectric gated, optoelectronic, etc.[4–7] Ferroelectric field effect transistors are regarded as ideal elements for nonvolatile memory devices because of their nonvolatility and precise polarization controllability under applied electric field.[8,9]

Compared to traditional inorganic ferroelectric materials like lead zirconate titanate (PZT) and $BaTiO_3$, the organic ferroelectric copolymer poly(vinylidene fluoride-trifluoroethylene) [P(VDF-TrFE)] requires lower crystallization temperatures.[10,11] Additionally, unlike two-dimensional inorganic ferroelectric materials such as α-In_2Se_3 and $CuInP_2S_6$, P(VDF-TrFE) can be directly integrated onto material surfaces via spin-coating, facilitating large-scale fabrication with excellent van der Waals contact.[12,13] In addition, the organic P(VDF-TrFE) films have excellent mechanical stability and flexibility, as well as transparency allowing the transmission of light when used as an gate control. These characteristics make it great potential for applications in storage, neuromorphic computing, optoelectronic and flexible wearable devices.[14–16]

The P(VDF-TrFE) polymers are extensively employed in gate control applications owing to their remarkable ferroelectric properties, including high residual polarization ($\sim 7\,\mu C/cm^2$), ultrafast switching capability($\sim 1\,\mu s$),[17] and compatibility with low-temperature processing, enabling effective modulation of semiconductor channel transport in diverse functional devices.[8,18] However, during the fabrication process of the gate/dielectric/semiconductor stack in an organic ferroelectric transistor, the organic solution utilized for the semiconductor layer deposition inevitably destroys P(VDF-TrFE) films, leading to substantial gate leakage currents.

Here, we insert an aluminum oxide (Al_2O_3) buffer layer on both sides of the P(VDF-TrFE) layer to improve its compatibility with other metals and organic semiconductors' deposition. We constructed ferroelectric neu-

†These authors contributed equally to this work.
*Corresponding author. Email: xjmeng@mail.sitp.ac.cn; x.guo@sjtu.edu.cn; bbtian@ee.ecnu.edu.cn
© 2025 Chinese Physical Society and IOP Publishing Ltd. All rights, including for text and data mining, AI training, and similar technologies, are reserved.

romorphic transistors by combining the organic polymer P(VDF-TrFE) and 6,13-Bis(triisopropylsilylethynyl) pentacene (TIPS-pentacene). The incorporation of alumina preserves P(VDF-TrFE) well during the following scraping and coating processes, effectively mitigating damage from chlorobenzene and evaporation electrodes. The carrier transport in the pentacene channel is effectively modulated through ferroelectric domain states in the Al_2O_3/P(VDF-TrFE)/Al_2O_3 multilayer. The device exhibits a large memory window of ∼24 V and excellent retention properties exceeding 600 s. Synaptic plasticity of long-term depression and potentiation has also been observed in this organic ferroelectric transistor. Additionally, an artificial neural network has been constructed for recognizing the Modified National Institute of Standards and Technology (MNIST) handwritten digit database and shows an accuracy of 92.8%.

The ferroelectric transistors in this work were fabricated on a SiO_2 substrate. Initially, patterned bottom electrodes composed of platinum (Pt), measuring 100 nm in thickness, were deposited onto a pristine SiO_2 substrate via magnetron sputtering. Then, atomic layer deposition (ALD) technology was employed to deposit an Al_2O_3 insulation layer with a thickness of ∼10 nm. The P(VDF-TrFE) films were prepared as follows: 2.5 g of P(VDF-TrFE) powder was weighed and dissolved in 100 mL of Diethyl Carbonate (DEC) solvent. The solution was then heated (60 ℃) in a water bath and stirred for 4 h to form a clear P(VDF-TrFE) solution, which was left to stand for 24 h after stirring and then prepared for use. A uniform P(VDF-TrFE) organic film was then created through the spin coating technique, and the growth of the ferroelectric β phase was facilitated through thermal annealing backing at 135 ℃ for 4 hours. Subsequently, another ∼10 nm Al_2O_3 layer was deposited following the same ALD process as the insulation layer. With the help of metal mask, thermal evaporation technology was utilized to deposit a 50 nm-thick silver (Ag) films as the source and drain electrodes. Then, self-assembled monolayer (SAM) modification was performed via deposition an isopropanol solution of per-fluorobenzenethiol onto the Ag source/drain electrodes for 15 minutes, followed by spin-coating at 1000 rpm for 60 seconds. The excess SAM material was rinsed off by spin-coating isopropanol at 1000 rpm for 60 seconds. The blended organic semiconductor solution of 10 mg/mL TIPS-pentacene and 10 mg/mL polystyrene in chlorobenzene (3:1 ratio by volume) was coated on a 70 ℃ substrate,[19] followed by backing at 100 ℃ for 10 minutes. Finally, a cyclic transparent optical polymer passivation layer was deposited on the sample via spin coating at a rate of 1000 rpm for 60 seconds, and then the sample was cured in a vacuum oven set to 65 ℃ for 20 minutes. The small molecule TIPS-pentacene is physically blended with a polymer material in solvent, and the polymer can not only promote organic semiconductor crystallization but also can work as a dopant by energy level matching to improve the electrical properties.[20]

The characteristic peaks of P(VDF-TrFE) were characterized using an X-ray diffractometer (XRD, D8 DISCOVER). The thickness of Al_2O_3 was measured via X-ray reflectometry (XRR, D8 DISCOVER). Piezoelectric force microscopy (PFM, Cypher) was employed to characterize the ferroelectricity of P(VDF-TrFE). Atomic force microscope (AFM, Cypher) was employed to measure the thickness of P(VDF-TrFE). The TF analyzer 3000 was utilized for characterizing the polarization versus voltage (P–V), transient current versus voltage (I–V), and fatigue characteristic curves of the device. A semiconductor parameter analyzer (Keithley 4200A-SCS) was used to test the retention characteristics, static I–V, and current versus time (I–T) electrical data of ferroelectric transistors.

The structure of the TIPS-pentacene ferroelectric field effect transistor (FeFET) with a Pt bottom gate structure is schematically shown in Fig. 1(a), in which Al_2O_3/P(VDF-TrFE)/Al_2O_3 serves as the gate insulator to provide nonvolatile ferroelectric polarization. The TIPS-pentacene channel is surfaced on the Ag source/drain electrodes, and the Ag-pentacene interface is reported to form a Schottky contact.[21] Figure 1(b) illustrates the optical image of the device, implying that the TIPS-pentacene, obtained through scraping, exhibits excellent crystallinity under the synergistic effect of SAM modification and silver coating. The channel width and length of the device are about 150 μm and 900 μm, respectively. Here, we choose the silver electrode as the source/drain electrode. Compared with gold and copper, silver exhibits relatively good stability and adhesion. The work function of silver can also match the HOMO level of p-type organic semiconductor (OSC) avoiding a large hole-injection barrier. In addition, silver is also cost-effective for large area applications. Figure 1(c) demonstrates the dual-sweep transfer characteristic curve of the typical TIPS-pentacene transistor by sweeping the bottom gate voltage (V_g) from +26 V to −26 V and back again with a fixed drain voltage V_{ds} = 1 V. The device exhibits good characteristics of a p-type semiconductor and a large memory window of ∼24 V. As shown in Fig. 1(c), the gate leakage current of our transistor is $\sim 4 \times 10^{-11}$ A. The operating energy consumption (E) of the device is related to the voltage amplitude (U), leakage current (I) and operating speed (t) of the device.[17,22] Therefore, according to the formula $E = UIt$, the operating energy consumption of the device can be estimated to be ∼1.2 fJ. The thicknesses of Al_2O_3 and P(VDF-TrFE) are determined using X-ray Reflectivity (XRR) (XRR technique can be used to measure the thickness of a thin film and is applicable to almost any thin film that has a different electron density compared to the substrate.) and AFM, respectively. Specifically, the thickness of Al_2O_3 deposited utilizing ALD with 100 cycles is checked by to be ∼10 nm, as shown in Fig. 1(d), while the thickness of P(VDF-TrFE) is checked by a step meter to be ∼150 nm, as depicted in Fig. 1(e). The XRD pattern of the P(VDF-TrFE) ferroelectric layer exhibits a distinct Bragg peak at 19.6° [Fig. 1(f)], which is characteristic of the ferroelectric β phase.[17,23]

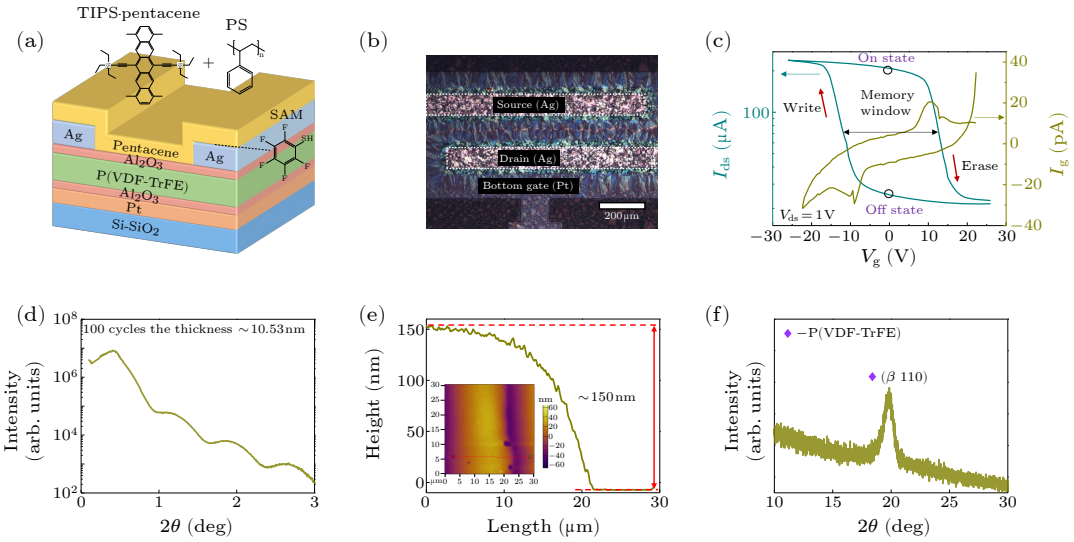

Fig. 1. (a) Schematics of the back-gate pentacene FeFET showing a pentacene thin film as the channel and Al_2O_3/P(VDF-TrFE)/Al_2O_3 as a gate insulation layer. (b) The optical image of the back-gate pentacene FeFET. (c) The dual-sweep transfer characteristic curve and gate leakage current of the pentacene FeFET. (d) The XRR pattern of Al_2O_3 films with 100 cycles using ALD. It gives a thickness of ∼10 nm. (e) The thickness of P(VDF-TrFE) films in Pt/Al_2O_3/P(VDF-TrFE)/Al_2O_3/Al novel ferroelectric capacitor is measured by AFM. (f) The XRD pattern of P(VDF-TrFE) films on Pt electrodes.

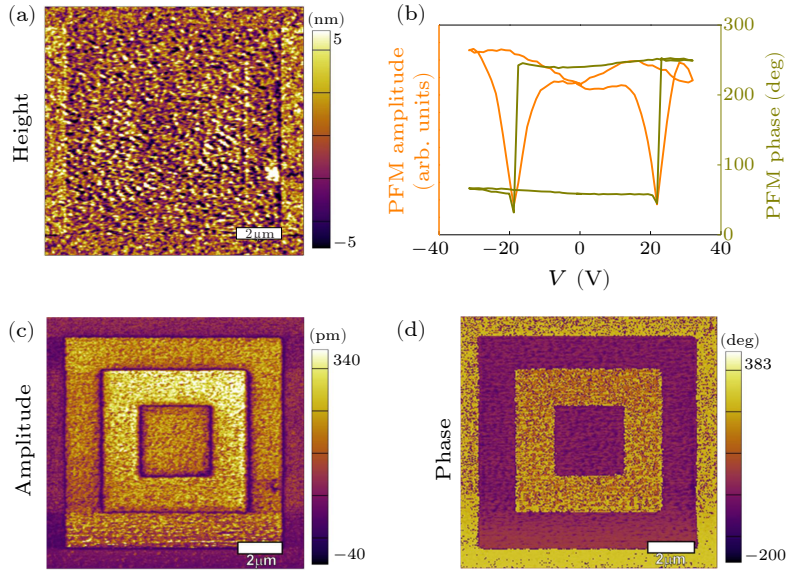

Fig. 2. (a) The PFM topographic image of the P(VDF-TrFE) films. The surface has a low average roughness of 2.18 nm across a $5 \times 5\,\mu m^2$ area. (b) The 180°-reversed PFM phase loop and butterfly-shaped piezoelectric PFM amplitude loop of P(VDF-TrFE) films on Pt electrodes. (c) and (d) The PFM amplitude image (c) and phase image (d) of the P(VDF-TrFE) films. Scale bar: 2 μm. The box-in-box ferroelectric domain pattern is written using +28 V and −28 V tip biases for downward and upward polarization respectively.

The PFM topographic image presented in Fig. 2(a) indicates that the P(VDF-TrFE) films display no significant macroscopic flaws, pinholes, or observable cracks. Additionally, these films have a root mean square roughness of approximately 2.18 nm, as derived from Fig. 2(a), which indicates that uniform and smooth P(VDF-TrFE) films are successfully obtained. The butterfly-shaped loop is observed in the PFM amplitude curves, as well as the 180°-reversed loop in the PFM phase curves, as shown in Fig. 2(b). By applying the ±28 V biases, ferroelectric domains and domain walls are clearly demonstrated as presented in Figs. 2(c) and 2(d) respectively. These PFM characteristics confirm the strong ferroelectric properties of the prepared P(VDF-TrFE) films.

Ferroelectric materials are known for its non-volatile and programmable properties.[22,24–26] Figure 3(a) presents the P–V hysteresis curve of the TIPS-pentacene FeFET based on P(VDF-TrFE), demonstrating its charac-

teristic polarization-electric field response, corresponding to multiple remnant polarization (P_r) states. The corresponding I–V curves are shown in Fig. 3(b), where the current peak due to polarization reversal becomes higher with increasing voltages, in agreement with the P–V hysteresis curves that higher voltage amplitude results in larger P_r value. Accordingly, by sweeping the gate voltage with positive amplitudes from 10 V to 26 V with a step of 2 V, as shown in Fig. 3(c), the TIPS-pentacene FeFET (V_{ds} = 1 V) shows nested transfer curves for nine different intermediate states due to the different polarization states of P(VDF-TrFE).[8,9] The retention characteristics of eight intermediate conductance states are measured, as shown in Fig. 3(d), demonstrating robust nonvolatile retention with slight degradation during 600 s period for all eight states.

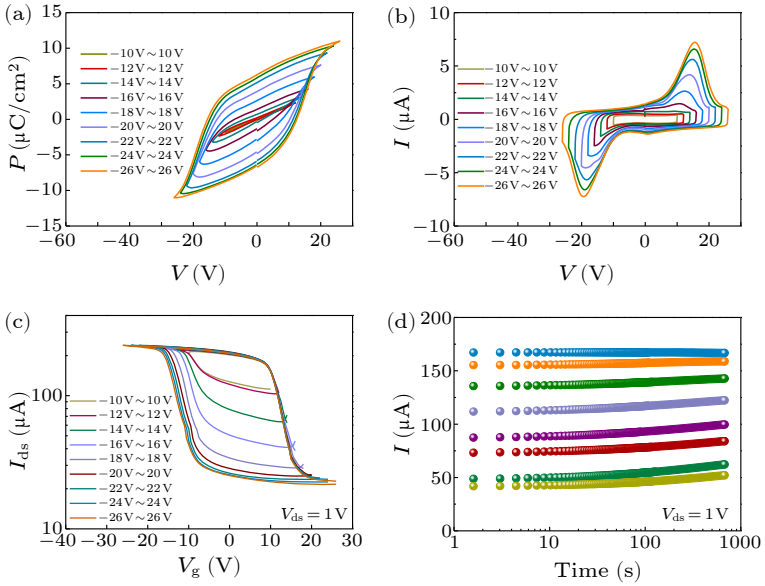

Fig. 3. (a) P–V hysteresis curves and (b) The I–V characteristics of the TIPS-pentacene FeFET, utilizing P(VDF-TrFE) films, were measured at a fixed sweeping frequency of 100 Hz. The voltage amplitude was progressively increased from 10 V to 26 V in 2 V increments. (c) The multiple quasi-static I_{ds}–V_g curves (V_{ds} = 1 V) in a logarithmic coordinate obtained by sweeping the gate voltage with positive amplitudes from 10 V to 26 V with a step of 2 V. (d) The retention characteristics of eight intermediate conductance states.

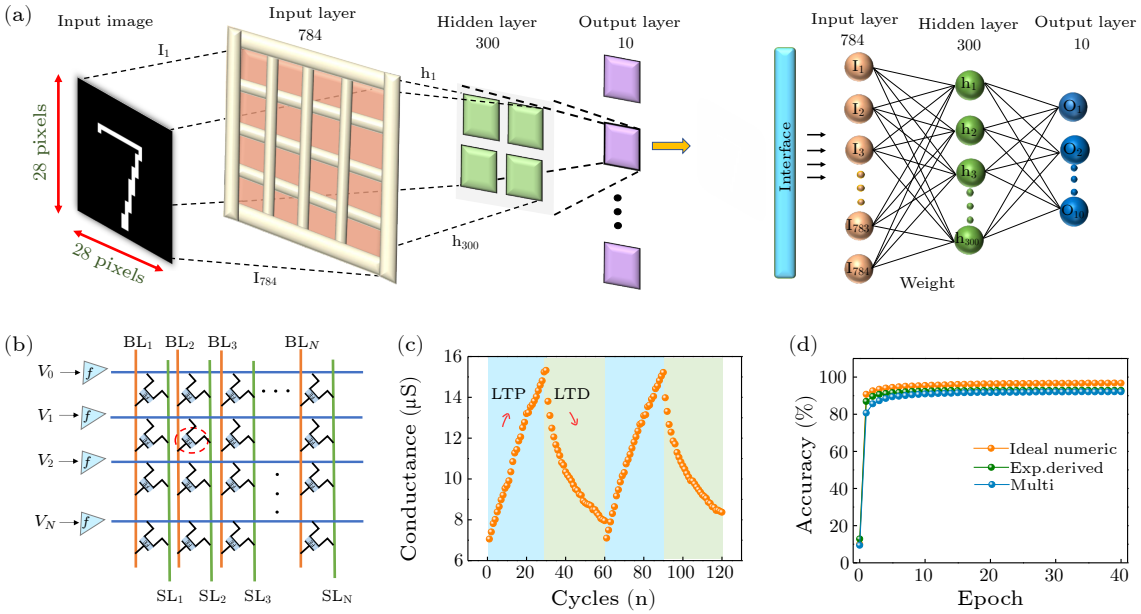

Fig. 4. (a) Schematic of the artificial neural network for recognizing handwritten digit images. (b) Proposed individual cell FeFET array. (c) The evolution of LTP and LTD during the polarization process, which involves a repetitive voltage pulse sequence consisting of 30 negative pulses (−15 V/100 ms) immediately followed by 30 positive pulses (+20 V/50 ms). (d) Training accuracy evolution of the neural network based on pentacene FeFET in 28 × 28-pixel image recognition.

Synaptic plasticity is the fundamental property of neuromorphic devices, which refers to the ability to regulate synaptic weights.[27,28] In memory and learning of biological systems, long-term depression (LTD: persistent decrease of synaptic weight) and long-term potentiation (LTP: persistent increase of synaptic weight) are regarded as the most fundamental functions.[29] In ferroelectric neuromorphic devices, the state of ferroelectric polarization is switched by applying multiple successive voltage pulses on the gate to obtain a controllable and stable conductance output. Figure 4(c) shows the dependence of LTP and LTD as a function of the number of gate voltage pulses, in which a series of commutative 30 negative pulses ($-15\,\mathrm{V}/100\,\mathrm{ms}$) and 30 positive pulses ($+20\,\mathrm{V}/50\,\mathrm{ms}$) were applied to the TIPS-pentacene FeFET and the conductance state was measured at $V_{\mathrm{ds}} = 1\,\mathrm{V}$ when each pulse is removed. With the evolution of ferroelectric domains modulated through external gate voltage pulses, LTP and LTD are obtained reproducibly.

Furthermore, the LTP and LTD properties of FeFETs can be used to simulate artificial neural networks. Handwritten digit images with 28×28 pixel inputs from the MNIST dataset are trained and recognized by different conductance states obtained in multi-pulse testing. For the simulation, a multilayer perceptron (MLP) neural network was employed using the Cross-Sim simulator [Fig. 4(a)]. This network comprises 784 input neurons, 300 hidden neurons, and 10 output neurons. The diagram in Fig. 4(b) illustrates a pentacene FeFET crossbar array used in a synaptic weight layer. In this setup, the pentacene FeFET crossbar array performs vector-matrix multiplication and outer-product update operations. For the digit images, our simulations show that the crossbar array with TIPS-pentacene FeFET can provide classification with 92.8% accuracy (green line), which remains 92.1% even after adding noise and device-device variables (blue line), as shown in Fig. 4(d). In summary, we can see that the TIPS-pentacene FeFET has potential in the field of neuromorphic computing.

In conclusion, Al_2O_3/P(VDF-TrFE)/Al_2O_3 is used as the gate dielectric layer to efficiently regulate the conductivity state of the pentacene channel by using ferroelectric polarization, which achieves a large memory window and retention characteristics. This organic ferroelectric neuromorphic transistor exhibits robust synaptic plasticity, including long-term potentiation/depression. The developed artificial neural network is used to recognize the MNIST handwritten digit database with 92.8% accuracy for a single device, and still 92.1% after adding noise and device-device variables. It is believed that the proposed organic ferroelectric neuromorphic transistor shows significant potential for the development of multifunctional neuromorphic computing systems.

Acknowledgements. This work was supported by the National Key Research and Development program of China (Nos. 2024YFA1410700 and 2021YFA1200700), the National Natural Science Foundation of China (Nos. T2222025, 62174053, 62474065 and 52372120), and the Natural Science Foundation of Chongqing (CSTB2024NSCQ-JQX0005), the Shanghai Science and Technology Innovation Action Plan (Nos. 24QA2702300 and 24YF2710400), the National Postdoctoral Program (GZB20240225) and the Fundamental Research Funds for the Central Universities.

References

[1] Rao M Y, Tang H, Wu J B, Song W H, Zhang M X, Yin W B, Zhuo Y, Kiani F, Chen B J M, Jiang X Q, Liu H F, Chen H Y, Midya R, Ye F, Jiang H, Wang Z R, Wu M C, Hu M, Wang H, Xia Q F, Ge N, Li J, and Yang J J 2023 *Nature* **615** 823

[2] Wan W E, Kubendran R, Schaefer C, Eryilmaz S B, Zhang W Q, Wu D B, Deiss S, Raina P, Qian H, Gao B, Joshi S, Wu H Q, Wong H S P, and Cauwenberghs G 2022 *Nature* **608** 504

[3] Zhang W B, Yao P, Gao B, Liu Q, Wu D, Zhang Q T, Li Y K, Qin Q, Li J M, Zhu Z H, Cai Y, Wu D B, Tang J S, Qian H, Wang Y and Wu H Q 2023 *Science* **381** 1205

[4] Cea C, Zhao Z F, Wisniewski D J, Spyropoulos G D, Polyravas A, Gelinas J N, and Khodagholy D 2023 *Nat. Mater.* **22** 1227

[5] Kamaei S, Liu X, Saeidi A, Wei Y F, Gastaldi C, Brugger J, and Ionescu A M 2023 *Nat. Electron.* **6** 658

[6] Li T X, Miao J S, Fu X, Song B, Cai B, Ge X, Zhou X H, Zhou P, Wang X R, Jariwala D, and Hu W D 2023 *Nat. Nanotechnol.* **18** 1303

[7] Marega G M, Zhao Y F, Avsar A, Wang Z Y, Tripathi M, Radenovic A, and Kis A 2020 *Nature* **587** 72

[8] Tian B B, Liu L, Yan M G, Wang J L, Zhao Q B, Zhong N, Xiang P H, Sun L, Peng H, Shen H, Lin T, Dkhil B, Meng X J, Chu J H, Tang X D, and Duan C G 2019 *Adv. Electron. Mater.* **5** 1800600

[9] Yan M G, Zhu Q X, Wang S Q, Ren Y M, Feng G D, Liu L, Peng H, He Y H, Wang J L, Zhou P, Meng X J, Tang X D, Chu J H, Dkhil B, Tian B B, and Duan C G 2021 *Adv. Electron. Mater.* **7** 2001276

[10] Dang Z Y, Guo F, Wu Z H, Jin K, and Hao J H 2023 *Adv. Phys. Research* **2** 2200038

[11] Yu R J, He L H, Gao C S, Zhang X H, Li E L, Guo T L, Li W W, and Chen H P 2022 *Nat. Commun.* **13** 7019

[12] Wang Y F, Zeng Z, Tian Z Q, Li C, Braun K, Huang L Y, Li Y, Luo X Y, Yi J L, Wu G C, Liu G X, Li D, Zhou Y, Chen M X, Wang X, and Pan A L 2024 *Adv. Mater.* **36** 2410696

[13] Zhu J Z, Wu S, Wang L M, Wu J Q, Zhu J K, Zou L W, Xiao F, Su Z L, Jiao C Y, Pei S H, Zhang Z J, Qin J Z, Xu B, Zhou Y, Xia J, and Wang Z H 2024 *Infomat* **6** e12553

[14] Guo M F, Jiang J Y, Qian J F, Liu C, Ma J, Nan C W, and Shen Y 2019 *Adv. Sci.* **6** 1801931

[15] Lee Y R, Trung T Q, Hwang B U, and Lee N E 2020 *Nat. Commun.* **11** 2753

[16] Feng G D, Zhao X M, Huang X Y, Zhang X X, Wang Y Y, Li W, Chen L Q, Hao S L, Zhu Q X, Ivry Y, Dkhil B, Tian B B, Zhou P, Chu J H, and Duan C G 2025 *Nat. Commun.* **16** 3027

[17] Feng G D, Zhu Q X, Liu X F, Chen L Q, Zhao X M, Liu J Q, Xiong S B, Shan K X, Yang Z Z, Bao Q Y, Yue F Y, Peng H, Huang R, Tang X D, Jiang J, Tang W, Guo X J, Wang J L, Jiang A Q, Dkhil B, Tian B B, Chu J H, and Duan C G 2024 *Nat. Commun.* **15** 513

[18] Tian B B, Xie Z Z, Chen L Q, Hao S L, Liu Y F, Feng G D, Liu X F, Liu H B, Yang J, Zhang Y Y, Bai W, Lin T, Shen H, Meng X J, Zhong N, Peng H, Yue F Y, Tang X D, Wang J L, Zhu Q X, Ivry Y, Dkhil B, Chu J H, and Duan C G 2023 *Exploration* **3** 20220126

[19] Huang Y K, Tang W, Chen S J, Han L, Hou X, and Guo X J 2019 *Ieee Electron Device Lett.* **40** 1945

[20] Paterson A F, Treat N D, Zhang W M, Fei Z P, Wyatt-Moon G, Faber H, Vourlias G, Patsalas P A, Solomeshch O, Tessler N, Heeney M, and Anthopoulos T D 2016 *Adv. Mater.* **28** 7791

[21] Hanic M, Vincze T, Rezo V, and Weis M 2024 *Synthetic Metals* **305** 117590

[22] Feng G D, Liu Y F, Zhu Q X, Feng Z Y, Luo S W, Qin C J, Chen L Q, Xu Y, Wang H N, Zubair M, Qu K, Yang C, Hao S L, Yue F Y, Duan C G, Chu J H, and Tian B B 2024 *Nat. Commun.* **15** 9701

[23] Tian B B, Bai X F, Liu Y, Gemeiner P, Zhao X L, Liu B L, Zou Y H, Wang X D, Huang H, Wang J L, Sun S, Sun J L, Dkhil B, Meng X J, and Chu J H 2015 *Appl. Phys. Lett.* **106** 092902

[24] Tian B B, Wang J L, Fusil S, Liu Y, Zhao X L, Sun S, Shen H, Lin T, Sun J L, Duan C G, Bibes M, Barthélémy A, Dkhil B, Garcia V, Meng X J, and Chu J H 2016 *Nat. Commun.* **7** 11502

[25] Wang D, Hao S L, Dkhil B, Tian B B, and Duan C G 2024 *Fundamental Research* **4** 1272

[26] Wu G J, Zhang X M, Feng G D, Wang J L, Zhou K J, Zeng J H, Dong D N, Zhu F D, Yang C K, Zhao X M, Gong D N, Zhang M R, Tian B B, Duan C G, Liu Q, Wang J L, Chu J H, and Liu M 2024 *Nat. Mater.* **23** 723

[27] Ham S, Kang M, Jang S, Jang J, Choi S, Kim T W, and Wang G 2020 *Sci. Adv.* **6** eaba1178

[28] Niu X Z, Tian B B, Zhu Q X, Dkhil B, and Duan C G 2022 *Appl. Phys. Rev.* **9** 021309

[29] Choi Y, Oh S, Qian C, Park J H, and Cho J H 2020 *Nat. Commun.* **11** 4595